International Journal of Electrical and Computer Engineering (IJECE)
Vol. 4, No. 3, June 2014, pp. 398~410
ISSN: 2088-8708

Two Novel Retinal Blood Vessel Segmentation Algorithms

Razieh Akhavan*, Karim Faez**
* Department of Computer Engineering, Gazvin branch, Islamic Azad University, Gazvin, Iran
** Electrical Engineering Department, Amirkabir University of Technology, Tehran, Iran

Article Info

Article history:

Received Feb 21, 2014
Revised May 4, 2014
Accepted May 20, 2014

Keyword:

Blood Vessel Segmentation
Morphological Operations
Neuro Fuzzy Classifier
Normalized Retinal Images

ABSTRACT

Assessment of blood vessels in retinal images is an important factor for many medical disorders. The changes in the retinal vessels due to the pathologies can be easily identified by segmenting the retinal vessels. Segmentation of retinal vessels is done to identify the early diagnosis of the disease like glaucoma, diabetic retinopathy, macular degeneration, hypertensive retinopathy and arteriosclerosis. In this paper, we propose two automatic blood vessel segmentation methods. The first proposed algorithm starts with the extraction of blood vessel centerline pixels. The final segmentation is obtained using an iterative region growing method that merges the contents of several binary images resulting from vessel width dependent modified morphological filters on normalized retinal images. In the second proposed algorithm the blood vessel is segmented using normalized modified morphological operations and neuro fuzzy classifier. Normalized morphological operations are used to enhance the vessels and neuro fuzzy classifier is used to segment retinal blood vessels. These methods are applied on the publicly available DRIVE database and the experimental results obtained by using green channel images have been presented and their results are compared with recently published methods. The results demonstrate that our algorithms are very effective methods to detect retinal blood vessels.

Corresponding Author:

Razieh Akhavan,
Department of Computer Engineering, Gazvin branch,
Islamic Azad University, Gazvin, Iran
Email: R.akhavan.a@gmail.com

1. INTRODUCTION

The diagnosis of the fundus image is widely used in many medical diagnoses. Image segmentation [1] in the fundus image is the important factor for identifying the retinal pathology. The analysis of the human retina helps the ophthalmologists to identify the retinal disease. The disease such as the diabetes, hypertension and arteriosclerosis affect the retina and cause the changes in the retinal blood vessels [2]. The changes in the blood vessel and the retinal pathology can be identified by first segmenting the retinal vessels and by proper analysis of the retinal blood vessels.

Automatic segmentation of retinal vessels is important for early diagnosis of eye diseases like diabetic retinopathy [3]. There are various segmentation methods for segmenting the retinal vessels in the fundus image which segments the retinal vessels using two dimensional matched filters and piecewise threshold probing [4, 5]. There are other segmentation processes which include segmentation of retinal vessels using the Mumford-Shah model and Gabor wavelet filter [6]. Extraction of retinal blood vessels is done using Weiner filter and the Morphological operations like open and close operation [7]. This paper focuses on segmentation of the retinal vessels to identify the changes in the retinal vessel which occurs due to retinal pathologies like diabetic retinopathy [8]. Vessel segmentation is done using Max-Tree to represent the image and the branches filtering approach to segment the image [9]. Mathematical morphology is mostly used for analyze the shape of the image. The two main processes which involve are dilation and erosion. The

algorithms of open and close are based on these processes. These algorithms are combined to detect the edges and identifying the specific shapes in the image and also for the background removal [10]. Retinal vessel segmentation is done to classify the pixel as the vessel and non-vessel using morphological thresholding. The retinal blood vessel is extracted by first smoothing the image and enhanced by applying the fuzzy c-means clustering algorithm [11].

2. METHODS

This paper proposes two novel algorithms for retinal blood vessels segmentation. The fundus image used in this research is obtained from Digital Retinal Images for vessel extraction (DRIVE database) [12]. The segmentation of the retinal blood vessel should be automatic and accurate for the diagnosis of the retinal disease. The first and second proposed algorithms and respective details will be explained here.

2.1. Overview of The First Proposed Algorithm

The method herein presented can be schematically described by the functional block diagram in Figure 1.

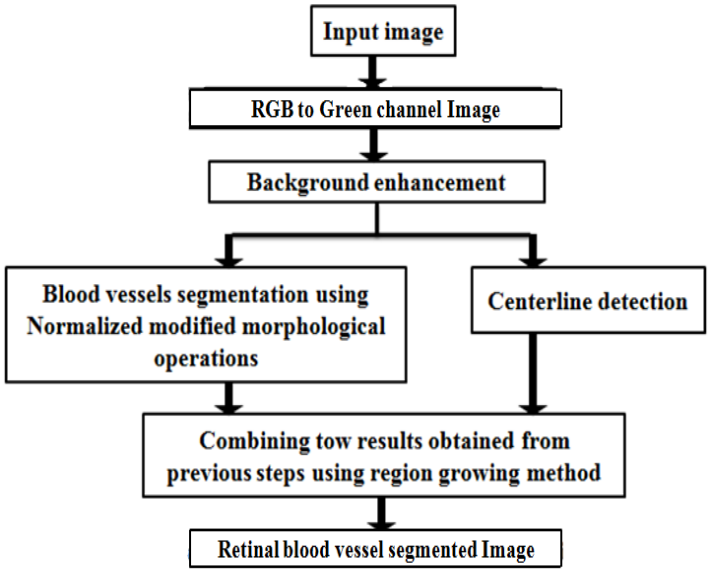

Figure 1. Retinal vessel segmentation functional diagram for first proposed algorithm

The algorithm consists three main processing parts: 1) preprocessing which includes background normalization and thin vessel enhancement using green channel of the retinal color images 2) vessel centerline detection and 3) vessel segmentation, to finally extract the pixels belonging to the retinal vessels. These parts are further subdivided in several steps.

2.1.1. Image Preprocessing

The background of retinal images have a gradual intensity variation and vessels are retinal structures that stand out from the background, but a more local analysis of vessel intensities can show significant changes that can negatively affect the complete vessel segmentation process. To decrease these negative influences, here we propose the modified Top-hat transform for the preprocessing step of our first proposed algorithm. And to improve the difference between thin vessels and the background noise, we also use a set of line detection filters for the green channel image obtained after applying the modified Top-hat operator.

2.1.1.1 RGB to Green Channel Conversion

The color fundus image is converted to green channel image to make the segmentation process more easily and to decrease the computational time. The green channel image provides the maximum contrast between the image and the background, because the retinal blood vessel information in the green channel image is more clear [13,14].

2.1.1.2 Modified Top-hat Transform

The classical top-hat transform is defined as the difference between an image and its opened version. A problem associated with this classical implementation is the sensitivity to noise, as a consequence of the fact that pixel values in an opened image are always less than or equal to the original ones; in such conditions, the different image retains all small intensity fluctuations that can be found in the data. To overcome this problem, a modification was adapted from [43], by considering two new steps in the top-hat definition: a closing precedes the opening result which is followed by a comparison, using a minimum operator, to get an image equal to the original one everywhere except for peaks and ridges. Equation (1) represents this modified top-hat transform, where I is the image to be processed, while Sc and So stand for the structuring elements for closing(•) and opening (***o***) operators, respectively[16].

$$\text{TopHat} = I - \min (I \bullet Sc) \; \boldsymbol{o} \; So \; ; I) \quad (1)$$

The closing operation is considered to generate a smooth version of the original data, where the details smaller than the structuring element are replaced by higher nearby intensities. The opened image essentially maintains the pixel values, while eliminating more intense image regions with sizes smaller than the structuring element size. The final result of the subtraction is an enhanced image that mostly retains the original image regions with size smaller than the structuring element which show significant local intensity variations.

Here we propose the modified Top-hat transform to produce the background normalized image. Figure 2(b) presents the background normalized image obtained with the modified top-hat operator.

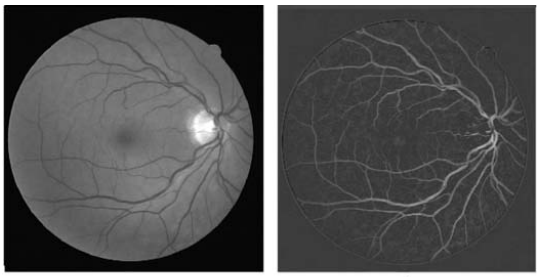

a **b**

Figure 2. a) Original Green Channel b) Background Normalized Image

Since thin vessels are very small structures and usually have low local contrast, their segmentation is a hard task. To improve the difference between these thin vessels and the background noise, we use a set of line detection filters [17], corresponding to the four orientations 0, 45, 90, and 135. These set of kernels used in this paper is shown in Figure 3. For each pixel, the highest filter response is kept and added to the background normalized image.

$$\frac{1}{6}\begin{bmatrix} -1 & -1 & -1 \\ 2 & 2 & 2 \\ -1 & -1 & -1 \end{bmatrix}; \quad \frac{1}{6}\begin{bmatrix} -1 & -1 & 2 \\ -1 & 2 & -1 \\ 2 & -1 & -1 \end{bmatrix}; \quad \frac{1}{6}\begin{bmatrix} -1 & 2 & -1 \\ -1 & 2 & -1 \\ -1 & 2 & -1 \end{bmatrix}; \quad \frac{1}{6}\begin{bmatrix} 2 & -1 & -1 \\ -1 & 2 & -1 \\ -1 & -1 & 2 \end{bmatrix}$$

Figure 3. Set of one-pixel width line detector filters used for thin vessel enhancement.

2.1.1.3 Detection of Centerline Segment Candidates

When a first-order derivative filter is applied orthogonally to the main orientation of the vessel, derivative values with opposite signs are created on the two vessel hillsides. This idea is shown in Figure 4(a) for an ideal vessel cross profile.

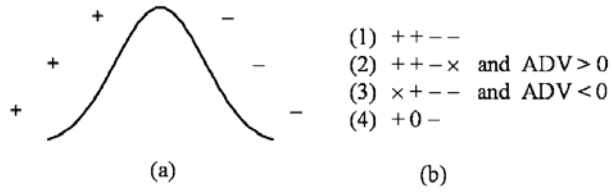

Figure 4. Ideal vessel profile with expected derivative signs on opposite hillsides. (b) Combinations of derivative signs and average derivative values that calculate the occurrence of a candidate centerline point: + means a positive derivative value;—means a negative value; 0 means a zero value; × is a do not care condition; ADV is the mean value of the derivative magnitudes obtained for the same set of four pixels were the specific combination of signs occurred [16].

As retinal vessels exist in any direction, we need to select a set of directional filters whose responses can be combined to cover the whole range of possible orientations. The particular kernels used in this work are first-order derivative filters, known as difference of offset Gaussians filters (DoOG filters), with common responses to horizontal (0), vertical (90), and diagonal (45,135) directions. These filters are used for the computation of the local image gradient in a specific direction. In fact, the DoOG filters have proved better immunity to noise because they depend on larger kernel derivative filters. Each filter is the difference between two displaced copies of a Gaussian whose scale specifies the DoOG kernel size [18].

Herein, the particular proposed kernels used for detecting centerline candidate pixels and the result of applying these filters are shown in Figure 5 and 6 respectively.

$$\begin{bmatrix} 0 & -1 & -2 & -1 & 0 \\ -1 & -2 & -4 & -2 & -1 \\ 0 & 0 & 0 & 0 & 0 \\ 1 & 2 & 4 & 2 & 1 \\ 0 & 1 & 2 & 1 & 0 \end{bmatrix} \begin{bmatrix} 0 & -1 & -2 & -1 & 0 \\ -1 & -4 & -2 & 0 & 1 \\ -2 & -2 & 0 & 2 & 2 \\ -1 & 0 & 2 & 4 & 1 \\ 0 & 1 & 2 & 1 & 0 \end{bmatrix} \begin{bmatrix} 0 & -1 & 0 & 1 & 0 \\ -1 & -2 & 0 & 2 & 1 \\ -2 & -4 & 0 & 4 & 2 \\ -1 & -2 & 0 & 2 & 1 \\ 0 & -1 & 0 & 1 & 0 \end{bmatrix} \begin{bmatrix} 0 & 1 & 2 & 1 & 0 \\ -1 & 0 & 2 & 4 & 1 \\ -2 & -2 & 0 & 2 & 2 \\ -1 & -4 & -2 & 0 & 1 \\ 0 & -1 & -2 & -1 & 0 \end{bmatrix}$$

Figure 5. The particular proposed kernels of the DoOG filter

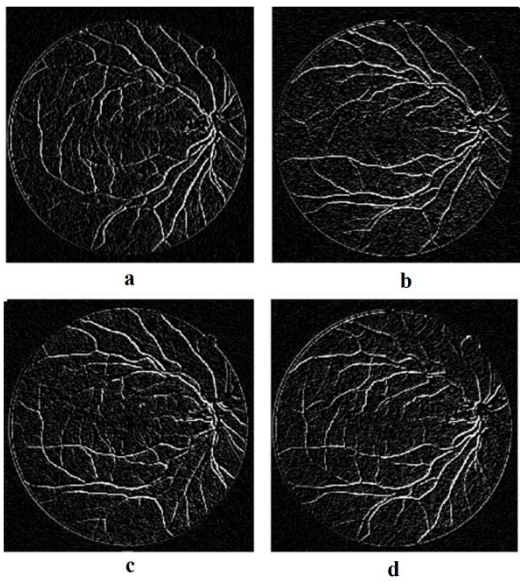

Figure 6. Selection of candidate centerline pixels by applying the proposed DoOG filters: a) vertical b) horizontal c) 135 d) 45.

Each one of the four directional images resulting from the proposed DoOG filters is searched for specific combinations of signs on the expected direction of the vessel cross section; Since real vessels do not have the ideal profile presented in Figure 4(a), a set of four combinations represented in Figure 4(b) that can find a vessel are used. In this figure, plus and minus signs show the positive and negative derivative responses, respectively, 0 means a null output, and × shows a do not care condition for the sign of the derivative. Moreover, in conditions 2 and 3, the average value of the derivative magnitudes (ADV) for the intensity profile is calculated. It must be positive for condition 2, and negative for condition 3[16]. The final centerline candidate is simply the pixel with the maximum intensity in the background normalized image. This fact is obtained in a new image by applying the sum of the highest positive response with the absolute value of the most negative response.

2.1.2. Vessel Segmentation

With the aim of achieving a complete segmentation, retinal vessels need to be filled starting from the detected centerlines. For this purpose, we propose a multiscale approach that uses a set of normalized morphological operators with increasing structuring elements size to generate several enhanced representations of the retinal vascular network. Each one of these images produces vessels in a particular width range, from smaller to larger vessels.

2.1.3. Normalized Mathematical Morphology

The Mathematical Morphology (MM) has been applied successfully to a large number of image processing problems. However, MM does not allow a complete representation of the uncertainties in images with high texture or a high degree of uncertainty in structural components [19]. The normalized images have several advantages to represent a better contrast enhancement in the images and turn out to be a useful tool for their segmentation. The MM operators can gain a much better result when applying on normalized images, there for we obtain normalized images and the morphological operations which are applied on the normalized images will be called Normalized Mathematical Morphology (NMM) for simplicity content.

In what follows I and SE denote two normalized sets, where the first corresponds to a grayscale image and the second is the structuring element. Importantly, for most cases the images in gray levels are defined so that the gray level intensity at each pixel is an integer value belonging to the natural range [0,255]. Therefore, we need to generate a function that changes the scale of these images, leading them to the range [0,1]. This process is called "Normalization". For the development of this work the normalization function $g:\{0,1,2\ldots,255\}\rightarrow[0,1]$ is proposed:

$$g(I)=(I-\min(I(:)))/\max(\max((I-\min(I(:)))))) \quad (2)$$

In which I(:) represents a column matrix made from all elements' intensities of image I.
Normalized dilation, erosion, close and open of the normalized image I by the normalized structuring element (SE) is given by:

$$(I\oplus SE) = \max (I(x-i,y-j) +SE(i,j))\ \ i,j\in SE \quad (3)$$

$$(I\ominus SE) = \min (I(x-i,y-j) +SE(i,j))\ \ i,j\in SE \quad (4)$$

$$I \bullet SE = (I \oplus SE) \ominus SE \quad (5)$$

$$I \circ SE = (I \ominus SE) \oplus SE \quad (6)$$

To obtain a multiscale representation of the retinal vascular structure, we apply a sequence of normalized modified Top-hat operators using circular structuring elements of increasing radius from 1 pixel to 8 pixels to the background normalized image. Here, Close is used to delete background noises, thus it is kept constant and equal to the smallest size of 1 pixel and pen is used to remove vessels with different sizes. Consequently, the radius of structuring element for the open is gradually increased. The average of the two images obtained by the application of operator with consecutive radii is computed, thus reducing the number of images with enhanced vessels to four.

The images obtained with the smallest structuring elements maintain the width for small vessels and larger structuring elements are able to extract larger vessels. Figure 7(a) represents the average of the images obtained with the circular structuring elements of 1 and 2, while the combination of the results using the structuring elements of 7 and 8 is shown in Figure 7(b).

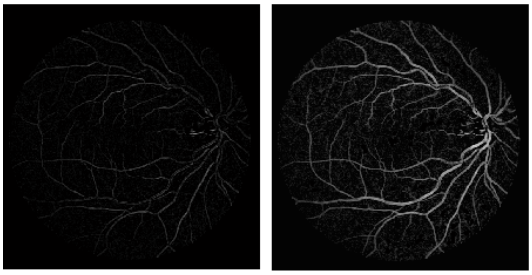

Figure 7. Outputs of the normalized modified top-hat operator for the image of Figure 5. (a) Result using circular structuring elements with radius 1 and 2. (b) Result using circular structuring elements with radius 7 and 8.

2.1.4. Vessel Segment Reconstruction

The four images resulting from the previous processing sequence are used for reconstructing potential vessel segments with the use of double threshold operator. This operator consists in thresholding each image for two ranges of gray values. For each one of the four images, we obtain the marker and mask images using threshold values derived from the intensity histogram of the non-null pixels; each one of the threshold is defined as the highest intensity value such that the number of pixels with intensities above this limit is greater or equal to a predefined percentage. The image obtained with the narrow threshold range is called marker image and used as a seed for the reconstruction using the wide range thresholded image, which is called mask image [20]. A correct selection of the marker and mask images allows the generation of four binary images, each one containing a partial reconstruction of the vascular tree of the retina.

Figure 8 shows the maker and mask images derived from the two Top-hat images of Figure 7. These results show the vessel width selectivity of the proposed approach. Finally, we calculate sum of these four binary images and the thin and thick vessels remain in a new binary image.

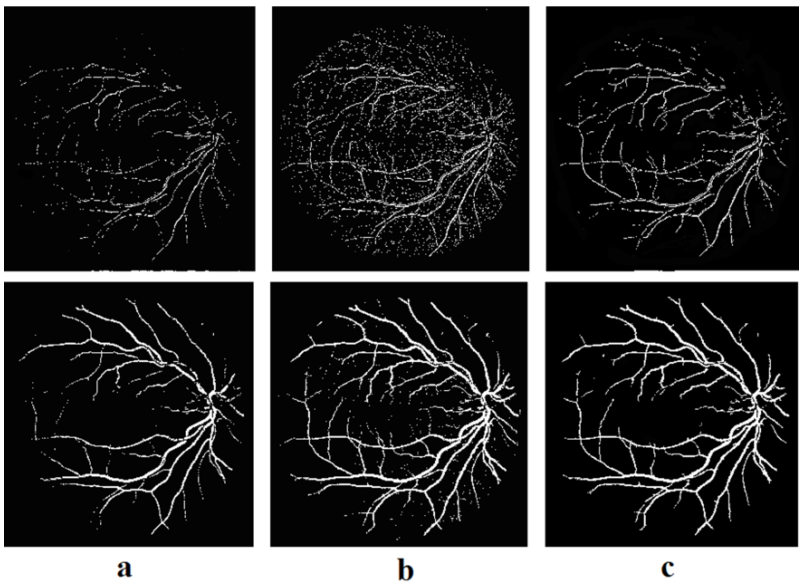

Figure 8. Morphological reconstruction operator for the enhanced images of Figure 7(a) (top row) and Figure 7(b) (bottom row). (a) Marker image. (b) Mask image. (c) Output of the morphological reconstruction operator.

2.1.5. Vessel Filling

The final image with the segmented vessels is obtained by iteratively combining the centerline image with the image that resulted from the vessel segments reconstruction part. Vessel centerline pixels are

used as primary points for a region growing algorithm, which fill these points by aggregating the pixels in the reconstructed image obtained from the normalized modified top-hat operator. Final result of the vessel filling part is illustrated in Figure 9.

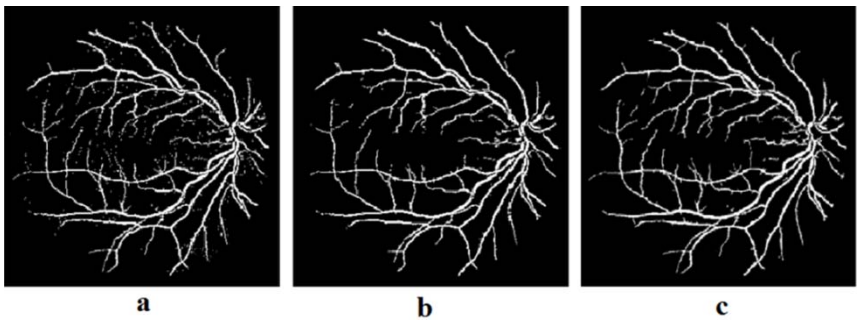

Figure 9. a) combination of the centerline image with the image that resulted from the vessel segments reconstruction part b) Image resulted from the vessel segments reconstruction part c) The final segmented image using region growing algorithm

2.2. Overview of The Second Proposed Algorithm

The method herein presented can be schematically described by the functional block diagram in Figure 10.

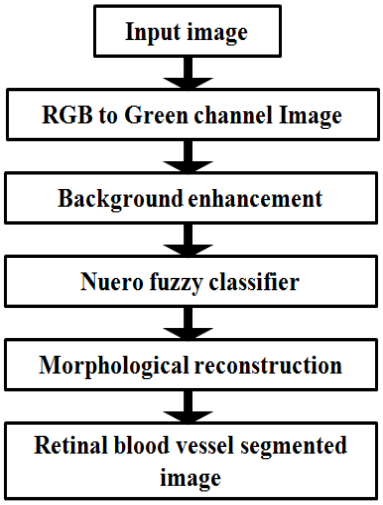

Figure 10. Retinal vessel segmentation functional diagram for second proposed algorithm

The main parts of the algorithm are: Color image (RGB) to green conversion, contrast enhancement, image segmentation, and double thresholding and background exclusion.

2.2.1. Color Image (RGB) to Green Conversion

As mentioned before, green channel of retinal images has the sharpest contrast for illustrating vessels and so vessel segmentation occurs on this channel of the image (refer to section 2.1.1.1).

2.2.2. Contrast Enhancement

Here we propose the operator normalized modified Top-hat which was previously explained. By implementing this operator to the green channel of the retinal images, an appropriate image is achieved for vessel segmentation (refer to sections 2.1.1.2 and 2.1.3). Implementation result of this operator is shown in the following image.

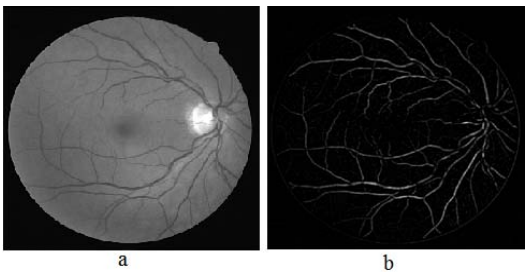

Figure 11. a) Original Green Channel b) Background Normalized Image

2.2.3. Image Segmentation

2.2.3.1. Neuro Fuzzy Classifier

The fuzzy classifier used is a self-organizing Takagi–Sugeno (TS)-type fuzzy network. The fuzzy classifier is used for object/non-object determination with color histograms as features [21]. Figure 12 shows the main structure. Each rule in (TS)-type fuzzy network is with TS-type and is of the following form:

Rule i: IF $x_1$is A_{i1} And … And x_n is A_{in} Then y'=$\sum_{j=1}^{v} p_{ij}\, x_j$ (7)

Where Aij is a fuzzy set and pij is a real number. The model of this five-layered network is described as follows:

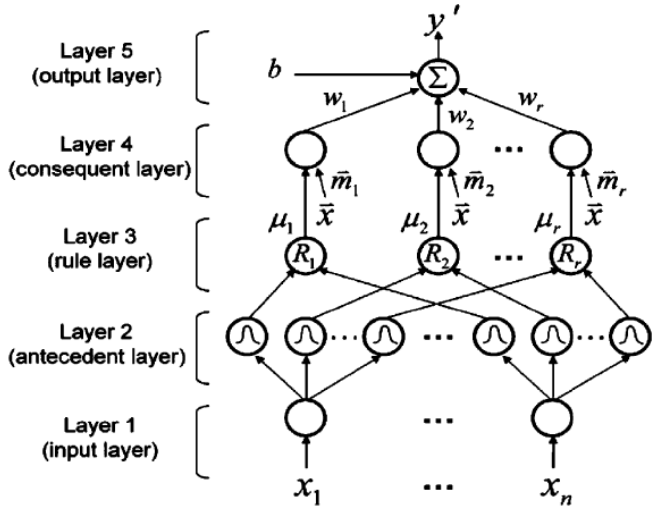

Figure 12. Structure of neuro fuzzy classifier

In Layer1, each node correspond stone input variable, and only transmits input values to the next layer directly. The training data is represented by a set S with.

S=$\{(\vec{x}_1, y_1), (\vec{x}_2, y_2) \ldots (\vec{x}_N, y_N)\}$ (8)

In Layer2, each node corresponds to a fuzzy set A and computes the degree to which an input value belongs to it. Fuzzy set Akj is employed with the following Gaussian membership function

$$M_{kj}(x_j) = \exp\{-\frac{(x_j - m_{kj})^2}{2\sigma_k^2}\} \quad (9)$$

Where mkj and σ_k denote the center and width of the fuzzy set, respectively. Here, for all the fuzzy sets connected to node k, the width is the same and is denoted as σ_k.

In Layer3, a node represents one fuzzy logic rule and performs an antecedent matching of a rule. The following AND operation is used for each node:

$$\mu_k(\vec{x}) = \prod_{j=1}^{n} M_{kj}(x_j) = \exp\{-\sum_{j=1}^{n}[\frac{(x_j - m_{kj})^2}{2\sigma_k^2}]\} = \exp\{-\frac{||\vec{x}-\vec{m}_k||^2}{2\sigma_k^2}\} \quad (10)$$

where $\vec{x} = [x_1, \ldots, x_n]$. Here the same width σ_k is assigned to all Gaussian fuzzy sets in the same rule.

Layer4 is called the consequent layer. For each node k, a linear combination of the inputs,i.e., $\vec{m}_k.\vec{x}$, is performed, where $\vec{m}_k$ is the center of the Gaussian fuzzy set in the antecedent part of the kth rule. The combination result of each node is then multiplied by its corresponding firing strength μ_k fromlayer3.Thus, the output value, O_k , of each node k in this layer is as follows:

$$O_k(\vec{x}) = \mu_k(\vec{m}_k.\vec{x}) = \exp\left\{-\frac{||\vec{x}-\vec{m}_k||^2}{2\sigma_k^2}\right\}(\vec{m}_k.\vec{x}) \quad (11)$$

where the output Q_k is the product of the Gaussian and linear functions. This function is a kernel function and is named TS-kernel [21]. The node number in layer4 is equal to the cluster number.

In Layer5, each node corresponds to one output variable. The node calculates the simple weighted sum for defuzzification. The node integrates all the actions recommended by Layer4 plus a bias. Thus, the output can be written as:

$$y' = \sum_{k=1}^{r} w_k Q_k(\vec{x}) + b = \sum_{k=1}^{r} w_k \exp\left(-\frac{||\vec{x}-\vec{m}_k||^2}{2\sigma_k^2}\right)(\vec{m}_k.\vec{x}) + b = \sum_{k=1}^{r} \exp\left(-\frac{||\vec{x}-\vec{m}_k||^2}{2\sigma_k^2}\right)(\vec{p}_k.\vec{x}) + b \quad (12)$$

where$\vec{p}_k = w_k\vec{m}_k$. Construction of neuro fuzzy classifier consists of antecedent and consequent learning parts. The antecedent part of neuro fuzzy classifier is generated via fuzzy clustering of the input data. A clustering threshold μ_{th} is used to determine the generated number of clusters, where a smaller value of μ_{th} generates a smaller number of rules. Detailed learning of neuro fuzzy classifier can be found in [21]. When neuro fuzzy classifier is trained as a classifier for object detection, there is only one output y in it. The desired output is set at ‘‘1’’and‘‘-1’’ when the inputs are histogram features of ‘‘object’’ and ‘‘non-object’’, respectively [22].

At first, the neuro fuzzy classifier is trained with 20 training images from the DRIVE database and then it is tested using all the database images. Figure 13 presents an example of vessel segmented image obtained with the neuro fuzzy classifier.

Figure 13. Vessel segmented image

2.2.3.2. Double Threshoulding and Background Exclusion

The threshold is applied on the extracted retinal vessels. After applying the threshold the background is eliminated and the properly segmented binary image of the retinal vessel is obtained. For this task, we selected double threshold operator (refer to section 2.1.3.2).

Figure 14 shows the maker and mask images and the output of the morphological reconstruction operator.

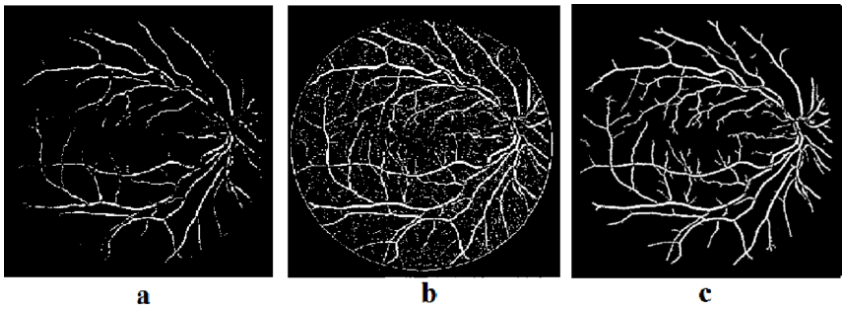

Figure 14. Result of morphological reconstruction operator a) Marker image b) Mask image c) Output of morphological reconstruction operator.

3. RESULT

Figure 15 shows the sample results of the segmentation process obtained from the fundus image taken from DRIVE database. To validate the vessel segmented image obtained by proposed algorithms, we used the gold standard image obtained from manual blood vessels segmentation by an expert. In Figure 15(a), the original image is shown, then part (b) shows the gold standard image obtained from manual blood vessels segmentation, Part c shows the image obtained using first proposed algorithm and finally Part d shows the segmented image using second proposed algorithm.

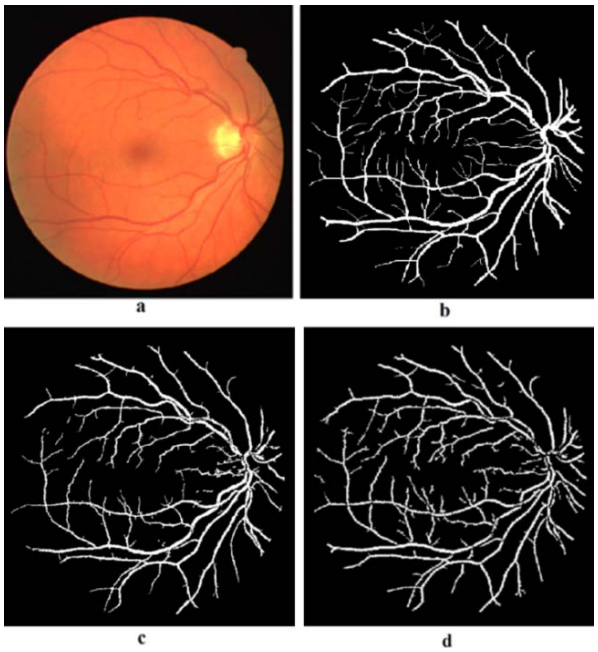

Figure 15. a) the original image b) gold standard image obtained from manual blood vessels segmentation c) segmented image using first proposed algorithm d) segmented image using second proposed algorithm

The evaluation results are given as the pixel-wise sensitivity, specificity, and accuracy of all the segmentation in comparison with ground truth, where sensitivity is a normalized measure of true positives, specificity measures the proportion of true negatives, and accuracy represents the proportion of the total number of correctly classified pixels relative to the total number of pixels.

$$\text{Sensitivity} = \frac{TP}{TP+FN}$$

$$\text{Specificity} = \frac{TN}{TN+FP}$$

$$\text{Accuracy} = \frac{(TP+TN)}{(TP+TN+FP+FN)}$$

True positive (TP) is a number of blood vessels correctly detected, false positive (FP) is a number of non-blood vessels which are detected wrongly as blood vessels, false negative (FN) is a number of blood vessels that are not detected and true negative (TN) is a number of non-blood vessels which are correctly identified as non-blood vessels.

Table 1 compares evaluation results of proposed methods with the listed approaches. In comparison with the listed methods, our first proposed method has the highest accuracy and specificity. In addition, it has the highest sensitivity compared to [23], [24] and [25]. Moreover, our second proposed algorithm has the highest accuracy, sensitivity and specificity in comparison with other listed methods.

Table 1. Average percentage of vessel segmentation methods

method	accuracy	sensitivity	specificity
First proposed method	95.42	71.25	98.96
Second proposed method	97.31	81.85	98.89
Baisheng Dai[23]	94.60	70.91	98.06
Espona[24]	93.16	66.34	96.82
Al-Diri[25]	92.58	67.16	_
Soares[26]	94.66	72.83	97.88
Vlachos[27]	92.85	74.68	95.51
Fraz[28]	94.30	71.52	97.68
Espona[29]	93.52	74.36	96.15
Mendonca[16]	94.52	73.44	97.64

4. CONCLUSION

We proposed two retinal blood vessel segmentation methods in this paper. The first technique is based on normalized modified morphological operations with different sizes and centerline detection and the second method is based on normalized modified top-hat transform and neuro fuzzy classifier. Our proposed vessel extraction techniques have consistent performance in both normal and abnormal images.

To validate the proposed methods we used images provided from the public database DRIVE, which includes the ideal segmentation, a tool necessary to carry out the validation of any method of segmentation. We could achieve the greatest specificity, accuracy and sensitivity, 95.42, 71.25 and 98.96 for the first proposed algorithm and 97.31, 81.85 and 98.89 for the second proposed algorithm.

REFERENCES

[1] A.K. Jain, *Fundamentals of digital image processing* vol. 3: Prentice-Hall Englewood Cliffs, 1989.
[2] L. Pedersen, M. Grunkin, B. Ersbøll, K. Madsen, M. Larsen, N. Christoffersen, *et al.*, "Quantitative measurement of changes in retinal vessel diameter in ocular fundus images," *Pattern Recognition Letters,* vol. 21, pp. 1215-1223, 2000.
[3] C. Sinthanayothin, J. Boyce, T. Williamson, H. Cook, E. Mensah, S. Lal, *et al.*, "Automated detection of diabetic retinopathy on digital fundus images," *Diabetic Medicine,* vol. 19, pp. 105-112, 2002.
[4] S. Chaudhuri, S. Chatterjee, N. Katz, M. Nelson, and M. Goldbaum, "Detection of blood vessels in retinal images using two-dimensional matched filters," IEEE Transactions on medical imaging, vol. 8, pp. 263-269, 1989.
[5] A. Hoover, V. Kouznetsova, and M. Goldbaum, "Locating blood vessels in retinal images by piecewise threshold probing of a matched filter response," *Medical Imaging, IEEE Transactions on,* vol. 19, pp. 203-210, 2000.
[6] X. Du and T.D. Bui, "Retinal image segmentation based on Mumford-Shah model and Gabor wavelet filter," in *Pattern Recognition (ICPR), 2010 20th International Conference on*, 2010, pp. 3384-3387.
[7] V.V. Kumari and N. Suriyanarayanan, "Blood vessel extraction using wiener filter and morphological operation," *Int. J. Comput. Sci. Emerg. Technol,* vol. 1, pp. 7-10, 2010.

[8] M. Foracchia, E. Grisan, and A. Ruggeri, "Extraction and quantitative description of vessel features in hypertensive retinopathy fundus images," in *Book Abstracts 2nd International Workshop on Computer Assisted Fundus Image Analysis*, 2001, p. 6.
[9] Y. Yang, S. Huang, and N. Rao, "An automatic hybrid method for retinal blood vessel extraction," *International Journal of Applied Mathematics and Computer Science,* vol. 18, pp. 399-407, 2008.
[10] N. Patton, T.M. Aslam, T. MacGillivray, I.J. Deary, B. Dhillon, R.H. Eikelboom*, et al.*, "Retinal image analysis: concepts, applications and potential," *Progress in retinal and eye research,* vol. 25, pp. 99-127, 2006.
[11] K. Noronha, J. Nayak, and S. Bhat, "Enhancement of retinal fundus Image to highlight the features for detection of abnormal eyes," in *TENCON 2006. 2006 IEEE Region 10 Conference*, 2006, pp. 1-4.
[12] M. Niemeijer, J.J. Staal, B.v. Ginneken, M. Loog, M.D. Abramoff, DRIVE: digital retinal images for vessel extraction, http://www.isi.uu.nl/Research/Databases/DRIVE,2004.
[13] A. Bouchet, M. Brun, and V. Ballarin, "Morfología Matemática Difusa aplicada a la segmentación de angiografías retinales," *Revista Argentina de Bioingeniería,* vol. 16, pp. 7-10, 2001.
[14] A. Bouchet, J.I. Pastore, and V.L. Ballarín, "Segmentation of medical images using fuzzy mathematical morphology," *Journal of Computer Science & Technology,* vol. 7, 2007.
[15] J. Gasparri, A. Bouchet, G. Abras, V. Ballarin, and J. Pastore, "Medical Image Segmentation using the HSI color space and Fuzzy Mathematical Morphology," in *Journal of Physics: Conference Series*, 2011, p. 012033.
[16] A.M. Mendonca and A. Campilho, "Segmentation of retinal blood vessels by combining the detection of centerlines and morphological reconstruction," *Medical Imaging, IEEE Transactions on,* vol. 25, pp. 1200-1213, 2006.
[17] W.K. Pratt, *Digital Image Processing*, 3rd ed. New York: Wiley, 2001.
[18] T.S. Yoo, G.D. Stetten, and B. Lorensen, "Basic image processing and linear operators," in Insight into Images, T. S. Yoo, Ed. Wesley, MA: A. K. Peters, 2004, pp. 19–45.
[19] J. Gasparri, A. Bouchet, G. Abras, V. Ballarin, and J. Pastore, "Medical Image Segmentation using the HSI color space and Fuzzy Mathematical Morphology," in Journal of Physics: Conference Series, 2011, p. 012033.
[20] P. Soille, *Morphological image analysis: principles and applications*: Springer-Verlag New York, Inc., 2003.
[21] C.F. Juang, S.H. Chiu, and S.W. Chang, "A self-organizing TS-type fuzzy network with support vector learning and its application to classification problems," *Fuzzy Systems, IEEE Transactions on,* vol. 15, pp. 998-1008, 2007.
[22] C.F. Juang, W.K. Sun, and G.C. Chen, "Object detection by color histogram-based fuzzy classifier with support vector learning," *Neurocomputing,* vol. 72, pp. 2464-2476, 2009.
[23] B. Dai, W. Bu, X. Wu, and Y. Teng, "Retinal vessel segmentation via Iterative Geodesic Time Transform," in *Pattern Recognition (ICPR), 2012 21st International Conference on*, 2012, pp. 561-564.
[24] L. Espona, M.J. Carreira, M. Ortega, and M.G. Penedo, "A snake for retinal vessel segmentation," in *Pattern Recognition and Image Analysis*, ed: Springer, 2007, pp. 178-185.
[25] B. Al-Diri, A. Hunter, and D. Steel, "An active contour model for segmenting and measuring retinal vessels," *Medical Imaging, IEEE Transactions on,* vol. 28, pp. 1488-1497, 2009.
[26] J.V. Soares, J.J. Leandro, R.M. Cesar, H.F. Jelinek, and M.J. Cree, "Retinal vessel segmentation using the 2-D Gabor wavelet and supervised classification," *Medical Imaging, IEEE Transactions on,* vol. 25, pp. 1214-1222, 2006.
[27] M. Vlachos and E. Dermatas, "Multi-scale retinal vessel segmentation using line tracking," *Computerized Medical Imaging and Graphics,* vol. 34, pp. 213-227, 2010.
[28] M.M. Fraz, P. Remagnino, A. Hoppe, B. Uyyanonvara, C.G. Owen, A.R. Rudnicka*, et al.*, "Retinal vessel extraction using first-order derivative of Gaussian and morphological processing," in *Advances in Visual Computing*, ed: Springer, 2011, pp. 410-420.
[29] B. Al-Diri, A. Hunter, and D. Steel, "An active contour model for segmenting and measuring retinal vessels," *Medical Imaging, IEEE Transactions on,* vol. 28, pp. 1488-1497, 2009.

BIOGRAPHIES OF AUTHORS

Razieh Akhavan, received her B.S. degree in software of computer Engineering from Lahijan Azad University as the first rank in May 2010, and now the student of M.S. degrees in Artificial Intelligence of Computer Science from Electrical and Computer Engineering Department of Islamic Azad University of Qazvin, Iran. Her research interests are in Pattern Recognition, Biometric Identification and Recognition, Image Processing, Neural Networks, Signal Processing, Farsi Handwritten Recognition.
Email: R.akhavan.a@gmail.com.

Karim Faez, received his B.S. degree in Electrical Engineering from Tehran Polytechnic University as the first rank in June 1973, and his M.S. and Ph.D. degrees in Computer Science from University of California at Los Angeles (UCLA) in 1977 and 1980, respectively. Prof. Faez was with Iran Telecommunication Research Center (1981-1983) before joining Amirkabir University of Technology in Iran. He was the founder of the Computer Engineering Department of Amirkabir University in 1989 and he has served as the first chairman during April 1989-Sept. 1992. Professor Faez was the chairman of planning committee for Computer Engineering and Computer Science of Ministry of Science, research and Technology (during 1988-1996). His research interests are in Pattern Recognition, Biometric Identification and Recognition, Image Processing, Steganography, Neural Networks, Signal Processing, Farsi Handwritten Recognition, Earthquake Signal Processing, Fault Tolerant System Design, Computer Networks. He is a member of IEEE, IEICE, and ACM. Emails: kfaez@aut.ac.ir, kfaez@ieee.org.